GMCL1 Controls 53BP1 Stability and Modulates Paclitaxel Sensitivity in Cancer

Yuki Kito[1,2], Tania J. González-Robles[1,3,4], Sharon Kaisari[1,2,4], Juhee Pae[1,2,5,#], Sheena Faye Garcia[1,2], Juliana Ortiz-Pacheco[1,2,6], Beatrix Ueberheide[1,2,6], Ruth Lehmann[5,^], Antonio Marzio[1,2,@], Gergely Rona[1,2,4,7,*] and Michele Pagano [1,2,4,9,*]

[1] Department of Biochemistry and Molecular Pharmacology, [2] Laura and Isaac Perlmutter Cancer Center, New York University Grossman School of Medicine, New York, NY 10016, USA

[3] Division of Precision Medicine, Department of Medicine, NYU Grossman School of Medicine, New York, NY 10016, USA

[4] Howard Hughes Medical Institute, NYU Grossman School of Medicine, New York, NY 10016, USA

[5] Department of Cell Biology, New York University Grossman School of Medicine, New York, NY 10016, USA

[6]Proteomics Laboratory, Division of Advanced Research Technologies, New York University Grossman School of Medicine, New York, NY 10016, USA

[7] Institute of Molecular Life Sciences, Research Centre for Natural Sciences, Budapest, 1117, Hungary.

[9] Lead contact

[#]Current address: Laboratory of Lymphocyte Dynamics, The Rockefeller University, New York, NY 10065, USA

^Current address: Whitehead Institute for Biomedical Research, Cambridge, MA 02142, USA

[@]Current address: Department of Pathology and Laboratory Medicine, Meyer Cancer Center, Weill Cornell Medicine, New York, NY 10065 USA

*Correspondence: rona.gergely@ttk.hu, michele.pagano@nyumc.org

KEYWORDS

GMCL1, prolonged mitosis, 53BP1, p53, mitotic stopwatch, protein degradation, ubiquitin

ABSTRACT

The Mitotic Surveillance Pathway (MSP) monitors the duration of M-phase. Prolonged mitosis, caused by spindle attachment defects or microtubule-targeting drugs such as the taxane paclitaxel, induces the formation of the ternary "mitotic stopwatch" complex consisting of 53BP1, USP28, and p53. This event protects p53 from degradation, resulting in cell cycle arrest or apoptosis in daughter cells. In paclitaxel-resistant cancers, cells bypass the MSP, enabling unchecked proliferation and survival, although the underlying mechanisms remain unknown. Here, we demonstrate that 53BP1 physically interacts with GMCL1 but not its paralog, GMCL2, and we mapped the interaction regions on both proteins. $CRL3^{GMCL1}$ functions as a ubiquitin ligase that targets 53BP1 for degradation during M phase, impacting p53 levels in daughter cells. High GMCL1 expression significantly correlates with resistance to paclitaxel in cancer cell lines with wild-type p53, including endometrial, breast, and upper aerodigestive tract cancer cells. Loss of GMCL1 restores paclitaxel sensitivity in p53 expressing cells but not in p53 deficient cells. We propose that in cancers with high GMCL1 levels, the $CRL3^{GMCL1}$-mediated degradation of 53BP1 prevents the formation of the mitotic stopwatch complex, leading to p53 degradation and sustained proliferation. Finally, our results indicate that GMCL1 inhibition represents a novel strategy to restore taxane sensitivity in resistant cancers.

INTRODUCTION

Mitosis is orchestrated by several intracellular signaling pathways to ensure proper cell division while maintaining genomic integrity. Errors during cell division, including chromosome mis-segregation or spindle defects, could lead to changes in chromosome content, producing aneuploid or polyploid progeny cells, which could be detrimental during development or lead to oncogenesis[1,2]. Therefore, cells have evolved quality control mechanisms to ensure proper cell division during M phase. One such surveillance mechanism is known as the Mitotic Surveillance Pathway (MSP), which senses prolonged mitosis as an indicator of mitotic defects[3].

If a threshold mitotic duration is surpassed, the MSP induces cell cycle arrest in the daughter cells in a p53-dependent manner[4-6]. During abnormally prolonged mitosis[7-10], the MSP is triggered by the formation of a ternary "mitotic stopwatch" complex consisting of the deubiquitinase USP28 (ubiquitin-specific protease 28), 53BP1 (p53-binding protein 1), which acts as a substrate recognition subunit, and p53. During delayed mitosis, formation of the mitotic stopwatch complex allows USP28 to deubiquitinate and subsequently protect p53 from MDM2-mediated degradation. The 53BP1-USP28-p53 complex accumulates and persists in the G1 phase of daughter cells, where it promotes cell cycle arrest *via* p53-mediated upregulation of p21 expression.

Notably, proper mitotic arrest plays a crucial role in the mechanism of microtubule-targeting therapies, such as taxanes (e.g., paclitaxel and docetaxel), which disrupt spindle formation and chromosomal segregation. Recent studies have shown that pharmacological interventions targeting M phase, even without resulting in complete mitotic arrest, can induce controlled cell death[11]. For example, low dose paclitaxel treatments results in increased p21 expression and apoptosis in daughter cells[12]. However, there are cancers that display resistance or insensitivity to treatment with taxanes, including metastatic breast cancer, ovarian cancer, and non-small cell lung cancer[13-15]. Therefore, there is an urgent need to elucidate the strategies of paclitaxel resistance in such cancers.

90 Human germ cell-less protein-like 1 (GMCL1) is a putative substrate receptor of one of
91 many CUL3-RING ubiquitin ligases (CRL3s). However, to date, GMCL1's biological role and
92 its substrates have remained uncharacterized. *GMCL1* received its namesake from its
93 *Drosophila melanogaster* homolog, *GCL* (Germ Cell-Less), which plays essential roles in
94 early embryonic development and germ cell determination[16,17]. *GMCL1*'s role in germ cell
95 development appears to have been evolutionarily conserved as loss of *GMCL1* expression in
96 mice has been shown to cause defects in meiosis and spermiogenesis[18], and altered *GMCL1*
97 expression was functionally associated with human asthenozoospermia[19]. Although *GMCL1*
98 homologs have been primarily associated with germ cell biology, several databases (e.g.,
99 GTEx[20] and GENT2[21]) indicate that *GMCL1* is expressed in somatic cells as well, suggesting
100 broader biological functions beyond germ cell development. In contrast, the GMCL1 paralog
101 GMCL2 is specifically expressed in germ cells.
102
103 Here, we present studies that shed light on the role of GMCL1 in somatic cells. We
104 demonstrate that, like its *D. melanogaster* counterpart, GMCL1 acts as a CRL3 substrate
105 receptor. We also identify 53BP1 as a *bona fide* substrate of $CRL3^{GMCL1}$, demonstrating that
106 its levels are regulated by GMCL1 during M phase. Reduction of mitotic 53BP1 by GMCL1
107 prevents the formation of the USP28-p53-53BP1 mitotic stopwatch complex and reduces
108 p53 transmission to daughter cells. We therefore propose that GMCL1 inhibition, in
109 combination with paclitaxel therapy, offers a promising strategy to overcome taxane
110 resistance.
111
112
113 **RESULTS**
114
115 **Identification of 53BP1 as an interactor of $CRL3^{GMCL1}$**
116 We have shown that the GMCL1 ortholog in *D. melanogaster*, GCL, is a substrate recognition
117 subunit of a CRL3 complex that is active specifically in mitosis[22]. So, we predicted the
118 human GMCL1 to also behave as a CRL3 substrate receptor. GMCL1 contains a BTB (Broad-
119 Complex, Tramtrack, and Bric-à-brac) and a BACK (BTB and C-terminal Kelch) domain
120 (**Supplementary Figure 1A**), consistent with other CRL3 receptors. On its C-terminus,

121 GMCL1 also contains a GCL domain (residues 379-515), which is distinct from the Kelch
122 domains commonly used by other CUL3 substrate receptors since it is predicted to form a
123 β-sandwich characterized by two opposing anti-parallel β-sheets, each made up of four β-
124 strands[22,23] (**Supplementary Figure 1A**). A Dali search[24] of GMCL1's C-terminal domain
125 reveals that it has some structural homology to the MATH (meprin and TRAF homology)
126 domain used by another CRL3 substrate receptor, SPOP[25], suggesting that the predicted
127 structure of GMCL1's GCL domain could also potentially act as a protein-protein interaction
128 motif to recruit substrates.
129
130 To investigate the role of GMCL1 in somatic cells, we used immunoprecipitation followed by
131 mass spectrometry (IP-MS) to identify binding partners of GMCL1. Proteomics studies were
132 performed by expressing and purifying the following FLAG-tagged proteins: (*i*) wild-type
133 GMCL1 (GMCL1 WT), (*ii*) GMCL1 E142K (GMCL1 EK), which carries a mutation in the BTB
134 domain that is predicted to disrupt its interaction with CUL3, and (*iii*) GMCL1 BTB/BACK-
135 only (GMCL1 BBO) that lacks the GCL domain (**Figure 1A-C**). IP-MS analysis identified
136 1,765 potential binding partners that specifically interact with GMCL1 *via* its C-terminal
137 domain. Using SAINT scores > 0.70 and FDR < 5%, this list was refined to 9 proteins that
138 showed significant interaction with GMCL1 WT and GMCL1 EK, but not with GMCL1 BBO,
139 with 53BP1 being the one of most enriched protein (**Figure 1B, Supplementary Table 1**).
140 This selective enrichment suggests that the C-terminal, "MATH-like" GCL domain of GMCL1
141 is critical for its interaction with binding partners, including 53BP1. The interaction
142 between GMCL1 and endogenous 53BP1 and CUL3 was validated using
143 immunoprecipitations (IPs) followed by immunoblotting (**Figure 1C,D**).
144
145 To further study the direct interaction between GMCL1 and 53BP1, we used AlphaFold 3[26]
146 to predict their binding interface and identify potential critical residues at the recognition
147 interface between the substrate receptor and 53BP1to see if mutating these residues could
148 abolish their interaction. Consistent with our initial IP-MS experiment, the Alphafold 3
149 model predicted that the C-terminal domain of GMCL1 would interact with 53BP1. Based
150 on the GMCL1-53BP1 complex structure prediction, we identified Arg 433, which appears
151 to be a solvent-exposed residue in GMCL1's GCL domain that could interact with 53BP1

152 without impeding GMCL1's binding to with CUL3. Thus, we generated the GMCL1 R433A
153 (GMCL1 RA) point mutant and tested its binding to 53BP1 using IP. As predicted, compared
154 to WT GMCL1, the R433A mutation completely abolished the binding of GMCL1 to 53BP1,
155 but did not impact GMCL1's binding to CUL3 (**Figure 1D**).
156
157 To determine which region of 53BP1 mediates its binding to GMCL1, we mapped the
158 predicted GMCL1-binding site on 53BP1 and identified a conserved IEDI amino acid
159 sequence within the Minimal Focus Forming region (MFF) of 53BP1[27] (**Supplementary**
160 **Figure 1B-E**). Through IPs, we demonstrate that a 53BP1 mutant either lacking the MFF
161 region or containing the IEDI-to-AAAA mutation within this region lost its interaction with
162 $CRL3^{GMCL1}$, suggesting that this conserved IEDI sequence within 53BP1's MFF forms a
163 critical degron recognized by GMCL1 (**Figure 1E**).
164
165 To examine the interaction between endogenous GMCL1 and endogenous 53BP1, we used
166 CRISPR-Cas9 to knock in a FLAG tag at the C-terminus of *GMCL1*. Immunoprecipitation
167 experiments confirmed that endogenous GMCL1 interacts with both endogenous CUL3 and
168 53BP1 (**Figure 1F**).
169
170 Finally, we sought to determine whether GMCL2, a GMCL1 paralog, is also able to interact
171 with 53BP1. Immunoprecipitation of FLAG-tagged GMCL1 or GMCL2 from HEK293T cells
172 revealed that while GMCL1 binds to 53BP1, GMCL2 does not (**Supplementary Figure 1F**),
173 suggesting that GMCL1 and GMCL2 have distinct functions.
174
175 Overall, our results suggest that GMCL1 is a *bona fide* CRL3 substrate receptor and interacts
176 specifically with 53BP1.
177
178 **GMCL1 loss leads to 53BP1 accumulations under prolonged M phase**
179 To investigate whether GMCL1 regulates 53BP1 stability, we generated *GMCL1* knock-out
180 (KO) cells using CRISPR Cas-9[28] and compared 53BP1 levels between *GMCL1* WT and two
181 *GMCL1* KO clones. We found that 53BP1 levels were significantly increased in our *GMCL1*
182 KO cells during M phase. While the whole cell extracts (WCE) showed modest differences

183 in GMCL1 levels between the *GMCL1* WT and KO clones, our fractionation experiments
184 revealed that 53BP1 mainly accumulated in the chromatin-bound fraction of *GMCL1* KO
185 cells (**Figure 2A**).
186
187 To further explore the role of GMCL1 on 53BP1 stability, we stably reconstituted U2OS
188 *GMCL1* KO cells with either GMCL1 WT or binding mutants (i.e., GMCL1 EK and GMCL1 RA).
189 Notably, the accumulation of 53BP1 in *GMCL1* KO cells was rescued only upon re-
190 expression of GMCL1 WT. In contrast, 53BP1 levels remained high in *GMCL1* KO cells
191 expressing either GMCL1 EK or GMCL1 RA (**Figure 2B**), emphasizing the importance of
192 GMCL1's ability to bind both CUL3 (through the E142 residue) and 53BP1 (through the
193 R433 residue) to regulate 53BP1 levels. Furthermore, GMCL1 WT re-expression in *GMCL1*
194 KO cells led to decreased mRNA levels of p21 and NOXA during mitosis, whereas the GMCL1
195 EK and GMCL1 RA mutants failed to suppress these transcripts (**Supplementary Figure**
196 **2A**).
197
198 Collectively, these findings indicate that GMCL1 modulates 53BP1 availability through
199 interactions with the $CRL3^{GMCL1}$ complex, playing a critical role in the regulation of 53BP1
200 levels in M phase.
201
202 During mitosis, 53BP1 has been implicated in monitoring centrosome integrity and mitotic
203 progression *via* the Mitotic Stopwatch Pathway (MSP). A recent study demonstrated that
204 cells experiencing abnormally prolonged mitosis transmit this information to daughter cells
205 though a ternary complex containing 53BP1, USP28, and p53 called the "mitotic stopwatch"
206 complex[7].
207
208 To investigate whether GMCL1 regulates this complex, we analyzed GMCL1 levels in post-
209 mitotic daughter cells seven hours after release from prolonged nocodazole arrest. *GMCL1*
210 KO daughter cells, reconstituted with GMCL1 WT, successfully re-entered the cell cycle,
211 exhibiting low levels of 53BP1, p53, and p21, along with reduced expression of apoptosis-
212 related genes (**Supplementary Figure 2B,C**). In contrast, cells reconstituted with either
213 the E142K or R433A mutant displayed persistently elevated levels of 53BP1, p53, and p21,

214 accompanied by increased expression of apoptosis-related genes (**Supplementary Figure**
215 **2B,C**). Notably, compared to parental cells, GMCL1 KO cells, whether reconstituted with WT
216 or mutant GMCL1 constructs, showed no significant alterations in cell cycle profiles
217 (**Supplementary Figure 2D**).
218
219 Next, we used cycloheximide (CHX) to inhibit translation and to assess the stability of
220 53BP1. We observed that in the chromatin-bound fraction of *GMCL1* KO cells, 53BP1 was
221 more stable compared to cells rescued with GMCL1 WT (**Figure 2C**).
222
223 These results suggest that cells lacking GMCL1 that experienced prolonged mitosis will
224 maintain elevated levels of p53, increasing the likelihood of apoptosis in subsequent cell
225 cycles.
226
227 **GMCL1 modulates paclitaxel resistance in cancer cells**
228 Paclitaxel, a widely used chemotherapeutic drug, stabilizes microtubules and prevents their
229 depolymerization, thereby halting cancer cell division and inducing apoptosis. To assess the
230 clinical significance of GMCL1, we investigated the relationship between GMCL1 expression
231 levels and Taxol resistance in various cancer cell lines. To this end, we leveraged the PRISM
232 (profiling relative inhibition simultaneously in mixtures) repurposing dataset, which
233 compiles the proliferation inhibitory activity of 4,518 compounds tested across 578
234 patient-derived cancer cell lines[29]. This high-throughput screening dataset provides
235 valuable insights into drug resistance mechanisms. We examined the impact of GMCL1
236 mRNA expression on Taxol resistance by analyzing taxane-related compounds from this
237 dataset, including cabazitaxel, docetaxel, and paclitaxel, integrating it with the Cancer
238 Dependency Map (https://depmap.org). Interestingly, we found that several cancer types
239 (*e.g.*: endometrial, breast, and upper aerodigestive tract cancers) with high levels of GMCL1
240 mRNA exhibited resistance to paclitaxel, cabazitaxel, and/or docetaxel (**Figure 3A-C**). In
241 contrast, lung cancer cell lines with high GMCL1 mRNA expression did not show such
242 tendencies (**Figure 3D**). Given that nearly half of lung cancers harbor p53 mutations[30], we
243 hypothesized that p53 status may influence GMCL1-mediated Taxol resistance. To further
244 investigate the functional relationship between GMCL1, 53BP1 and p53 in Taxol resistance,

245 we stratified cancer cells based on their p53 status (wild-type vs mutant) and analyzed
246 GMCL1 mRNA expression and 53BP1 protein levels. In cancer cells with wild type p53, high
247 GMCL1 mRNA expression and low 53BP1 protein levels correlated with significant
248 increased resistance to Cabazitaxel and Paclitaxel when compared to cells with low GMCL1
249 mRNA and high 53BP1 protein levels (**Figure 3E**). However, this effect was abolished in
250 p53-mutant cells, where GMCL1 status no correlated with Taxol resistance (**Figure 3F**).
251
252 To further verify the impact of GMCL1 levels on Taxol sensitivity, we performed cell viability
253 and apoptosis assays using cells with wild type or mutant p53. In p53 wild-type cells
254 (MCF7 and U-2OS), Taxol treatment led to a significant reduction in cell viability and an
255 increase in apoptosis in GMCL1-depleted cells compared to cells transfected with non-
256 targeting control siRNA (**Figure 4A-D**). However, GMCL1 knockdown did not affect cell
257 viability or apoptosis in Taxol-treated cells with mutant p53 or inactivated p53 (HeLa and
258 HEC-1-A, respectively) (**Figure 4E-H**).
259
260 These observations are consistent with the results shown in Figure 3 and support the
261 hypothesis that Taxol resistance is mediated by GMCL1 through the USP28-p53-53BP1
262 complex. Specifically, high GMCL1 expression promotes the degradation of 53BP1,
263 maintaining low p53 levels, thereby reducing Taxol-induced cell death in cell that have
264 functional p53.
265
266
267 **DISCUSSION**
268 We identify GMCL1, a previously uncharacterized human CRL3 substrate receptor, as a
269 regulator of taxane resistance. Specifically, we found that GMCL1 interacts with and
270 mediates the degradation of 53BP1 during prolonged arrest in M phase. While 53BP1 is
271 well known for its role in double-strand break (DSB) repair via non-homologous end
272 joining (NHEJ)[31], it also participates to a so-called mitotic stopwatch composed of the
273 53BP1-USP28-p53 complex that stabilizes p53 during prolonged mitotic arrest[7-9]. We
274 showed that GMCL1 controls the levels of 53BP1 and, consequently, those of p53 in mitotic
275 cells, thereby influencing p53 transmission to daughter cells (see model in **Figure 4I**). This

data suggests that GMCL1 functions as a mitotic stress regulator, with potential oncogenic properties in certain contexts.

Cancer database analysis reveals that GMCL1 is overexpressed in multiple cancers, including bladder, brain, breast, kidney, liver, lung, ovary, prostate, skin, and stomach cancers (**Supplementary Figure 3**). This underscores GMCL1's role in mitotic regulation and genomic stability, which may vary based on tumor type, genetic background, and additional oncogenic mutations. Recent studies indicate that the MDM2-p53 axis[10], along with the USP28-53BP1-p53 complex, functions as a mitotic timer enforcing G1 arrest following prolonged cell division. Our study identifies GMCL1 as an E3 ligase regulating this pathway by mediating 53BP1 degradation in mitosis. As often is the case for crucial regulatory proteins, 53BP1 is subject to regulation by multiple factors under different cellular circumstances[32-34].

GMCL1 has been primarily studied in the germ cells of *D. melanogaster*, where we have shown that it forms an active CRL3 complex during mitosis. Our new findings establish a critical role for GMCL1 in somatic cell fate decisions by regulating 53BP1 stability during prolonged mitosis. We found that GMCL1 loss enhances Taxol-induced cell death in p53 wild-type cancers but has no effect in p53-mutant cells (**Figure 4I**). This suggests that GMCL1 inhibition could be selectively effective in cancers that retain functional p53. These findings position GMCL1 as a key modulator of mitotic stress and Taxol resistance, highlighting its potential as a therapeutic target in cancer treatment.

DATA AND CODE AVAILABILITY

- Original western blot images have been deposited at Mendeley at DOI:10.17632/gj3x6r263d.1 and are publicly available as of the date of publication. https://data.mendeley.com/preview/gj3x6r263d?a=1e452dfc-bf85-472c-83ce-0e997ba6fa40

305 • The mass spectrometric raw files are accessible at https://massive.ucsd.edu under
306 accession MassIVE MSV000097235 and at www.proteomexchange.org under accession
307 PXD061458. Username: MSV000097235_reviewer, Password: TP53bdg-protein1
308

309 **ACKNOWLEDGMENTS**

310 We would like to thank the NYU Proteomics Lab (supported in part by NYU School of
311 Medicine and the Laura and Isaac Perlmutter Cancer Center Support grant P30CA016087
312 from the National Cancer Institute). We also thank the members of the Pagano Lab for
313 helpful discussions. MP is an investigator with the Howard Hughes Medical Institute and his
314 laboratory is supported by grant R35-GM136250 from the NIH. Y.K. is a recipient of the
315 Japan Society for the Promotion of Science (JSPS) Postdoctoral Fellowships and the Uehara
316 Memorial Foundation Postdoctoral fellowship. T.G.R. is grateful for funding from NIH
317 Institutional training grant in Cell Biology (T32GM136542) and HHMI Gilliam Fellowship
318 (GT15758). A. M is supported by US Department of Defense (DoD) (HT9425-24-1-0019).
319 S.K. is a recipient of the Life Sciences Research Foundation (LSRF) Postdoctoral Fellowship
320 and has been an EMBO Long Term Postdoctoral Fellow. G.R. is supported by the
321 Momentum Grant of the Hungarian Academy of Sciences (LP2023-15/2023), EMBO
322 Installation Grant (IG5670-2024) and the HUN-REN Welcome Home and Foreign
323 Researcher Recruitment Grant (KSZF-143/2023).
324
325

326 **AUTHOR CONTRIBUTIONS**

327 Y.K., G.R. and M.P. conceived, supervised, and coordinated the study. T.G.R. performed all
328 analyses from PRISM and DepMap data. Y.K. performed the mass spectrometric sample
329 preparation, generated CRISIPR KO and KI cell lines, designed plasmid constructs, and
330 performed the cell-based immunoprecipitations, fractionation and protein stability assays.
331 A.M. and J.P. performed the initial mass spectrometric sample preparation and
332 immunoprecipitations. B.M.U and J.O.P performed mass spectrometry analysis. S.F.G.
333 performed structural predictions using AlphaFold3. The manuscript was written with
334 inputs from all authors.
335

336

337 **DECLARATION OF INTERESTS**

338 MP is or has been an advisor for SEED Therapeutics, CullGen, Deargen, Kymera
339 Therapeutics, Lumanity, Serinus Biosciences, Sibylla Biotech, Triana Biomedicines, and
340 Umbra Therapeutics. He also has financial interests in CullGen, Kymera Therapeutics, SEED
341 Therapeutics, Thermo Fisher Scientific, and Triana Biomedicines. The other authors
342 declare no conflict of interest.

343

344 **MATERIALS AND METHODS**

345 **Cell culture**

346 Cell lines were purchased from ATCC and were routinely checked for mycoplasma
347 contamination with the MycoStrip Mycoplasma Detection Kit (Invivogen). HEK293T (ATCC
348 CRL-3216), HeLa (ATCC CCL-2) were maintained in Dulbecco's modified Eagle's medium
349 (DMEM) (Gibco). U-2 OS (ATCC HTB-96), HCT-116 (ATCC CCL-247) and HEC-1-A (ATCC
350 HTB-112.NM) cells were maintained in McCoy's 5A medium (Gibco). MCF7 (ATCC HTB-22)
351 were maintained in Eagle's Minimum Essential Medium (EMEM) (ATCC). All media were
352 supplemented with 10% fetal bovine serum (FBS) (Corning Life Sciences) and 1%
353 penicillin/streptomycin/L-glutamine (Corning Life Sciences); however, MCF7 was further
354 supplemented with 0.28% human recombinant insulin, zinc solution (11.2 μg/ml, Gibco).
355 All cell lines were maintained at 37 °C and 5% CO2 in a humidified atmosphere.
356

357 **Plasmids, siRNA, and transfection**

358 *Homo sapiens* cDNAs were amplified by PCR using KAPA HiFi DNA Polymerase (Kapa
359 Biosystems) and sub-cloned into a variety of vector backbones, including modified
360 pCDNA3.1 vectors containing C-terminal Flag tags, and pLVX-PURO lentiviral vectors
361 containing C-terminal Flag. Site-directed mutagenesis was performed using KAPA HiFi DNA
362 Polymerase (Kapa Biosystems). All cell lines were transiently transfected using
363 Lipofectamine 3000 (ThermoFisher Scientific) based on the manufacturer's
364 recommendation. siRNA oligo transfections were performed using RNAiMax
365 (ThermoFisher Scientific) according to the manufacturer's instructions.
366

367 **Virus-mediated gene transfer**

368 For the generation of lentivirus, HEK293T cells were transfected with pLVX constructs
369 carrying the genes of interest, alongside the packaging plasmids pCMV-delta-R8.2 and
370 pCMV-VSV-G. Viral supernatant was harvested 48 hours post-transfection, passed through
371 a 0.45-μm sterile Millex-HV filter unit (Millipore Sigma), and supplemented with polybrene
372 at a final concentration of 8 μg/ml (Sigma). Target cells were infected by replacing their
373 culture medium with the virus-containing supernatant for an 8-hour incubation period.

374 Selection of successfully transduced cells was performed using puromycin at a
375 concentration of 1–2 μg/ml (Sigma).
376
377 **CRISPR-Cas9 genome editing**
378 CRISPR–Cas9 genome editing techniques were carried out as previously described[35] with
379 modifications. In brief, to generate *GMCL1*-knockout U-2 OS cells, optimal gRNA target
380 sequences closest to the start codon of the genes were designed using the Benchling
381 CRISPR Genome Engineering tool (https://www.benchling.com). For transient Cas9
382 expression, gRNAs specific for *GMCL1* gene was incorporated into the pRP [CRISPR]-Hygro-
383 hCas9-U6 vector, which was obtained from VectorBuilder (https://en.vectorbuilder.com/).
384 The following oligos were used to generate the proper gRNA in the vector: GMCL1 (5'-
385 CGTGCCCCCACGTACCTTCG-3'). To generate *GMCL1* 2×Flag knock-in HCT116 cells, an
386 optimal gRNA target sequence closest to the genomic target site and a ~2 kb homologous
387 recombination (HR) donor template was designed using the Benchling CRISPR Genome
388 Engineering tool. The HR donor template was designed to introduce a 2×Flag tag in frame
389 with the C terminus of *GMCL1*, in the following order: GMCL1-linker-FLAG-linker-FLAG-
390 Stop codon and was purchased from VectorBuilder (https://en.vectorbuilder.com/). The
391 following single gRNA sequence was used for the transient hCas9 expression vector: GMCL1
392 (5'-AAGTTACAGCAGATATATAA-3').
393 Genomic DNA was collected using QuickExtract (Epicentre). Genotyping PCRs were
394 performed with MyTaq HS Red Mix (Bioline), using primers surrounding the genomic
395 target sites. The following primers were used for genotyping: GMCL1 (F: 5'-
396 GCAGGCTTCTGATCTTCCCT-3', R: 5'-ACTTGTCATCGTCGTCCTTGT-3'), and GMCL1 (F: 5'-
397 GGGTGGGAGTTTGGAGAGTG-3', R:5'-TCTGGATTTTCTGGGTGACGA-3'). The resulting PCR
398 products were then purified and sequenced to determine the presence of insertion or
399 deletion events. Clones positive to insertion or deletion events were then validated by
400 western blot.
401
402 **Antibodies**
403 The following antibodies were used: β-actin (1:5,000, Sigma-Aldrich A5441), CUL3
404 (1:1,000, Bethyl Laboratories A301-109A), FLAG (1:2,000, Sigma-Aldrich F7425), GMCL1

405 (1:1,000, Proteintech 15575-1-AP), HA (1:2,000, Bethyl Laboratories A190-108A), Histone
406 H3 (1:1,0000, Abcam, ab1791), p21 (1:1,000, Cell Signaling Technology 2947S), p53
407 (1:1,000, Proteintech 10442-1-AP), pHistone H3 (D2C8) (Ser10, 1:1,000, Cell Signaling
408 Technology, #3377), USP28 (1:1,000, Proteintech 17707-1-AP), 53BP1 (1:2,000, Abcam
409 ab36823), α-tubulin (1:5,000, Sigma-Aldrich T6074).
410
411 **Drug treatment procedures**
412 Where indicated, cells were treated with 0.4 mg/ml Nocodazole (Sigma-Aldrich M1404) for
413 16 hours, 10 μM MG132 for 3 hours, 2.5 μM MLN4924 for 3 hours, 100 μg/ml
414 cycloheximide (CHX) for the indicated time.
415
416 **qRT-PCR**
417 Total RNA was purified using RNeasy mini kits (Qiagen). cDNA was generated using Double
418 Primed EcoDry kits (Takara). The qPCR reaction was carried out using PowerUp SYBR
419 Green (Applied Biosystems) and the Applied Biosystems QuantStudio 3 Real-Time PCR
420 system in a 96-well format. ROX was used as a reference dye for fluorescent signal
421 normalization and for well-to-well optical variations correction. Bar graphs represent the
422 relative ratios of target genes to β-actin housekeeping gene values. For each biological
423 sample, triplicate reactions were analyzed using absolute relative quantification method
424 alongside in-experiment standard curves for each primer set to control for primer
425 efficiency. The oligos used for qRT-PCR analysis were: β-actin (F: 5'-
426 CATGTACGTTGCTATCCAGGC-3', R: 5'-CTCCTTAATGTCACGCACGAT-3'), GMCL1 (F: 5'-
427 GGAGATTCCTGACCAGAACATTG-3', R: 5'-CGACTGGGCTTTATCAAGACAT-3), GMCL2 (F: 5'-
428 CCACGCAGCGGGTCTGT, R: 5'-TGGATTTTCTGGGTGACGATTATTT), p21 (F: 5'-
429 TGTCCGTCAGAACCCATGC-3', R: 5'-AAAGTCGAAGTTCCATCGCTC-3'), NOXA (F: 5'-
430 CCAAGCCGTGACCAAGGAC-3', R: 5'-CGCCACATTGTGTAGCACCT-3'), PUMA delta (F: 5'-
431 GCCAGATTTGTGAGACAAGAGG-3', R: 5'- CAGGCACCTAATTGGGCTC-3').
432
433 **Immunoprecipitation, immunoblotting, and fractionation**

434 For whole-cell lysates, cells were directly lysed in a buffer containing 25 mM Tris-HCl (pH
435 8.0), 150 mM NaCl, 0.2% NP-40, 10% glycerol, 1 mM EDTA, 1 mM EGTA, 2 mM $MgCl_2$, 1 mM
436 dithiothreitol (DTT), and 5 mM N-ethylmaleimide (Sigma-Aldrich). When cellular
437 fractionation was performed, it followed a previously established method[36]. Briefly, cells
438 were lysed in CSK buffer (10 mM PIPES, pH 7.0, 150 mM NaCl, 300 mM sucrose, 0.1%
439 Triton X-100, 3 mM $MgCl_2$, 1 mM EGTA, 1 mM DTT, and 5 mM N-ethylmaleimide) for 5
440 minutes. The soluble fraction was collected by centrifugation at 3,000 × g for 3 minutes at
441 4°C. Cell pellets were subsequently washed in CSK buffer and then lysed in chromatin
442 extraction buffer (50 mM Tris-HCl, pH 7.5, 150 mM NaCl, 0.2% NP-40, 10% glycerol, 1 mM
443 EDTA, 1 mM EGTA, 4 mM $MgCl_2$, 0.5 mM DTT, 5 mM N-ethylmaleimide, and 5 U/mL
444 TurboNuclease (Accelagen)) for 30 minutes. Insoluble debris was removed by
445 centrifugation at 20,000 × g for 15 minutes at 4°C. All buffers were supplemented with
446 protease inhibitors (Complete ULTRA, Roche) and phosphatase inhibitors (PhosSTOP,
447 Roche).
448
449 For immunoprecipitation and affinity purification, samples were incubated with FLAG-M2
450 magnetic beads (Sigma-Aldrich) at 4°C for 2 hours. Beads were thoroughly washed with
451 lysis buffer, and protein elution was performed using either FLAG peptide (Sigma-Aldrich)
452 for mass spectrometry analysis or 1x Laemmli sample buffer for Western Blot analysis.
453
454 **Immunoblotting**
455 Western blotting was carried out as described previously[35]. Protein samples were resolved
456 under denaturing and reducing conditions on 4%–12% Bis-Tris gels (NuPAGE) and
457 transferred onto PVDF membranes (Immobilon-P, Millipore). Membranes were blocked
458 with 5% nonfat dried milk, incubated overnight at 4°C with primary antibodies, followed by
459 washes and incubation with HRP-conjugated secondary antibodies (Amersham GE).
460 Immunoreactive bands were visualized using enhanced chemiluminescence reagents
461 (Pierce) and detected with a ChemiDoc MP imaging system (Bio-Rad). Each Western blot
462 experiment was conducted at least three times to ensure reproducibility, with
463 representative blots shown in the figures.
464

465 **Cell cycle analysis by flow cytometry**

466 BrdU incorporation and propidium iodide staining were performed following established
467 protocols[37]. In brief, cells were pulse-labeled with 10 μM BrdU (Merck) for 45 minutes,
468 followed by trypsinization and overnight fixation in ice-cold 70% ethanol. After washing
469 with PBS and subsequently with PBST-BSA (1% BSA, 0.5% Tween-20 in PBS), DNA
470 denaturation was carried out for 30 minutes using 2 N HCl with 0.5% Triton X-100. The
471 cells were then washed in PBS and neutralized by resuspending them in 0.1 M sodium
472 tetraborate (pH 8.5) for 2 minutes. To detect BrdU incorporation, cells were incubated for 1
473 hour at room temperature with FITC-conjugated anti-BrdU mouse antibodies (BD
474 Transduction Laboratories, 556028) in PBST-BSA. After multiple washes, cells were
475 resuspended in PBST-BSA containing 5 μg/mL propidium iodide (Invitrogen) and 20
476 μg/mL RNase A (Invitrogen). Flow cytometry analysis of cell cycle distribution was
477 conducted using a CytoFlex Analyzer (Beckman Coulter) and data were processed with
478 FlowJo v10 software (Becton Dickinson).

479

480 **Mass spectrometry analysis of GMCL1 immunoprecipitations**

481 The eluted anti FLAG-tag antibody purified protein complexes were reduced with 2 μl of 0.2
482 M DTT for 1 h at 57 °C and subsequently alkylated with 2 μl of 0.5 M iodoacetamide (Sigma)
483 for 45 min at room temperature in the dark. 250 ng of SP3 beads (Cytiva) were added
484 proteins precipitated onto the beads by adding ethanol. Samples were placed in a
485 thermomixer at 25°C for 10 min. Beads were washed three times with 80% ethanol and
486 then digested overnight with 400ng of sequencing grade modified Trypsin (Promega) in
487 100 mM ammonium bicarbonate. Next, the samples were spun down 21,000 x g for 1
488 minute. The supernatant was transferred to a new tube while the beads were washed twice
489 with 0.5% acetic acid. The washes were then combined with the supernatant collection.
490 Samples were acidified with 10% TFA to pH1 and loaded onto a 0.1% TFA equilibrated
491 Pierce C18 spin column using a microcentrifuge. The samples were rinsed twice with 0.1%
492 TFA and twice more using 0.5% acetic acid. Peptides were eluted with 80% acetonitrile in
493 0.5% acetic acid. The organic solvent was removed using a SpeedVac concentrator and the
494 sample reconstituted in 0.5% acetic acid.

495

496 An equal aliquot of each sample was loaded onto a trap column (Acclaim PepMap 100 pre-
497 column, 75 µm × 2 cm, C18, 3 µm, 100 Å, Thermo Scientific) connected to an analytical
498 column (EASY-Spray column, 50 m × 75 µm internal diameter, PepMap RSLC C18, 2 µm,
499 100 Å, Thermo Scientific) using the autosampler of an Easy nLC 1200 (Thermo Fisher
500 Scientific) with solvent A consisting of 2% acetonitrile in 0.5% acetic acid and solvent B
501 consisting of 80% acetonitrile in 0.5% acetic acid. The peptide mixture was gradient eluted
502 using the following gradient: 5% solvent B for 5 minutes, 5–35% solvent B in 60 min, 35–
503 45% solvent B in 10 min, followed by 45–100% solvent B in 10 min. The samples were
504 acquired on the Orbitrap Eclipse using the following parameters: full MS spectra resolution
505 of 120,000, an AGC target of 4e5, maximum ion time of 50 ms, scan range from 400 to 1,500
506 m/z. The MS/MS spectra were collected with the following parameters: a resolution of
507 30,000, an AGC target of 2e5, maximum ion time of 30 ms, one microscan, 2 m/z isolation
508 window, normalized collision energy (NCE) of 27 and a dynamic exclusion of 30 s. To
509 identify binding partners, all acquired MS2 spectra were searched against a UniProt human
510 database using Sequest HT within Proteome Discoverer 1.4 (Thermo Fisher Scientific).
511 Fixed modifications were set on cysteine (carbamidomethyl), variable modifications of
512 oxidation on methionine, and deamidation on glutamine and asparagine. The resulting
513 peptide spectra matches and proteins are filtered to better than 1% false discovery rate
514 (FDR) and only proteins with at least two different peptides are reported. Proteins
515 differentially expressed between GMCL1 WT and EK, as determined by SAINT scores with a
516 5% FDR, were considered significantly enriched interactions when comparing to GMCL1
517 BTB.
518
519 **Taxol resistance analysis**
520 Taxol resistance was analyzed across cancer cell lines catalogued in DepMap 24Q2. We
521 integrated TP53 mutation status, *GMCL1* RNA and *TP53BP1* protein expression information
522 across cells with the PRISM dataset[29], to evaluate taxol resistance in the context of *GMCL1*
523 or *TP53BP1* levels and *TP53* mutation.
524
525 **Cell viability and apoptosis assays**

526 Cells (2500/well) were plated in a 96-well plate. The medium was replaced with 50 μL of
527 medium containing the target siRNA (0.2 μL/well). After 24 hours, an additional 50 μL of
528 the designated reagent was added. Luminescence was measured using BioTek Synergy
529 Neo2 (Agilent) 48 hours post-treatment with CellTiter-Glo 2.0 Cell Viability Assay
530 (Promega) or RealTime-Glo Annexin V Apoptosis and Necrosis Assay (Promega) according
531 to the manufacturer's protocol.
532
533 **Quantification and statistical analysis**
534 Data analysis was performed using GraphPad Prism version 10.2.1. For comparisons
535 involving three or more groups, One-way ANOVA followed by Bonferroni's post hoc test or
536 the Brown-Forsythe and Welch ANOVA test followed by Dunnett'S T3 multiple comparisons
537 test was applied. For bioinformatic data analysis, two-group comparisons were performed
538 using the pairwise Wilcoxon rank-sum test.
539

540 **FIGURE LEGENDS**

541

542 **Figure 1. Identification of 53BP1 as a GMCL1 interactor**

543 A) Schematics for the immunoprecipitation-mass spectrometry (IP-MS) workflow
544 using wild-type GMCL1 (GMCL1 WT) and mutants (GMCL1 EK and GMCL1 BBO).
545 Color coding: Red, GMCL1; orange, putative substrates/interacting partners; blue,
546 CUL3; green, RBX1; purple, E2 ubiquitin-conjugating enzyme.

547 B) HEK293T cells were transfected with FLAG-GMCL1 WT, FLAG-GMCL1 EK, or FLAG-
548 GMCL1 BBO. After 24 hours, FLAG-tagged proteins were immunoprecipitated and
549 analyzed by MS/MS. Left panel: proteins enriched with GMCL1 WT vs. BBO; right
550 panel: proteins enriched withGMCL1 EK vs. BBO. Significant interactors were
551 identified using SAINT scores > 0.70 and FDR < 5%.

552 C) HEK293T cells transfected with empty vector (EV), FLAG-GMCL1 WT, FLAG-GMCL1
553 BBO, FLAG-GMCL1 WKE_AAA (broadly disrupts the binding to CUL3) and FLAG-
554 GMCL1 EK were treated with MLN4924 (3h). 53BP1 and CUL3 were
555 immunoprecipitated with FLAG beads and analyzed by western blot. Asterisk
556 indicates non-specific bands.

557 D) HEK293T cells were transfected with EV, FLAG-GMCL1 WT, FLAG-GMCL1 EK, or
558 FLAG-GMCL1 RA. FLAG immunoprecipitations were probed for 53BP1 and CUL3.

559 E) HEK293T cells were transfected with EV, FLAG-53BP1 WT, FLAG-53BP1 ΔMFF and
560 FLAG-53BP1 IEDI_AAAA. After MLN4924 treatment (3h), GMCL1 was
561 immunoprecipitated and immunoblotted.

562 F) M phase-synchronized GMCL1 FLAG knock-in HCT116 cells were collected. GMCL1
563 was immunoprecipitated using FLAG-beads and analyzed by immunoblotting.

564

565 **Figure 2. GMCL1 targets 53BP1 for degradation during M phase**

566 A) Asynchronous or M phase-synchronized WT or GMCL1 knockout (KO) U2OS cells
567 were collected. Whole-cell extracts (WCE) were prepared using RIPA buffer, and
568 other lysates were fractionated into soluble and chromatin-bound fractions for
569 immunoblotting. Arrow indicates GMCL1-specific bands. Asterisk indicates non-
570 specific bands.

571 B) Stable U2OS cell lines expressing EV, FLAG-GMCL1 WT, FLAG-GMCL1 EK, or FLAG-
572 GMCL1 RA in a GMCL1 KO background were synchronized into M phase and
573 fractionated for chromatin immunoblotting.
574 C) Mitotic-synchronized FLAG-GMCL1-expressing cells were collected by shake-off and
575 cultured in fresh FBS-containing medium for 7 h. Daughter cells were treated with
576 CHX at the indicated time points and collected within 7 hours, fractionated into
577 soluble and chromatin-bound fractions, and analyzed by immunoblotting.
578
579 **Figure 3. GMCL1 expression shows positive correlation with Taxol resistance in**
580 **cancel cell lines**
581 For each cancer type (A-D) and p53 status (E-F), two visualization methods are
582 presented:
583 Upper panels: Density plots show the distribution of drug responses (log2[cell
584 viability]) to the indicated taxane. Each curve represents the frequency of cell lines
585 exhibiting specific response values. Blue curves represent high GMCL1 expression,
586 while orange curves show low GMCL1 expression. Vertical dashed lines indicate
587 median response values for each group. Rightward shifts of blue curves (high
588 GMCL1) indicate greater resistance.
589 Lower panels: Boxplots of the same data showing median (horizontal line),
590 interquartile range (box), and distribution range (whiskers). Higher values on the y-
591 axis indicate greater resistance to the drug. Statistical significance is indicated (*$p <$
592 0.05; ns: not significant) using Wilcoxon rank-sum test.
593 In panels E-F, cell lines are stratified by both GMCL1 mRNA and 53BP1 protein levels
594 as 'Low_High' (low GMCL1/high 53BP1, red) or 'High_Low' (high GMCL1/low
595 53BP1, green). Note the significant differences in panels E (wild-type p53) but not in
596 panels F (mutant p53), demonstrating that GMCL1-mediated taxane resistance
597 requires functional p53 signaling.
598
599 **Figure 4. GMCL1 deficiency sensitizes cancers with wild-type p53 to Taxol-induced**
600 **apoptosis**

601 MCF7 (A), U2OS (C), HeLa (E), HEC-1-A (G) cells were transfected with GMCL1-
602 targeting siRNAs or non-targeting (NT) control for 72 h. Cells were treated with
603 DMSO or Taxol for 48 h, and cell viability was assessed using the CellTiter-Glo Cell
604 Viability Assay. Error bars represent standard deviation. Apoptosis was measured in
605 the same conditions, i.e., MCF7 (B), U2OS (D), HeLa (F), HEC-1-A (H), using the
606 RealTime-Glo Annexin V Apoptosis and Necrosis Assay. Error bars represent
607 standard deviation.
608 (I) Overview of GMCL1's function during the M phase. In cancers with high GMCL1
609 levels, the $CRL3^{GMCL1}$-mediated degradation of 53BP1 prevents the formation of the
610 mitotic stopwatch complex, leading to p53 degradation and sustained proliferation.
611 Loss of GMCL1 stabilizes mitotic 53BP1 levels and restores paclitaxel sensitivity.
612
613
614 **SUPPLEMENTAL FIGURE LEGEND**
615
616 **Supplemental Figure 1. Mapping 53BP1 binding sites on GMCL1**
617 (A) Predicted structure of GMCL1, domain architecture overview, and comparative
618 analysis of the substrate-binding domain across Drosophila, fish, chicken, mouse,
619 and human. Conserved amino acids are indicated by asterisks, with the human R433
620 residue highlighted in red.
621 (B) Schematic representation of 53BP1 domains.
622 (C) HEK293T cells were co-transfected with FLAG-GMCL1 and either EV, HA-53BP1 WT,
623 or deletion mutants: HA-53BP1 ΔMFF, HA-53BP1 ΔN (lacking the N-terminus of
624 MFF), HA-MFF, HA-MFF ΔOD (oligomerization domain), HA-MFF ΔGAR (glycine-
625 arginine-rich motif), HA-MFF Δ1270-1484, or HA-MFF Δ1370-1484.
626 Immunoprecipitation of 53BP1 was performed using HA beads, followed by
627 immunoblotting of co-purified proteins.
628 (D) HEK293T cells were transfected with EV or FLAG-GMCL1, together with HA-53BP1
629 WT or mutants: HA-MFF, HA-53BP1 ΔMFF, HA-53BP1 ΔN (lacking the N-terminus of
630 MFF), HA-53BP1 ΔTudor, and HA-53BP1 ΔC (lacking the C-terminus of MFF). 53BP1

631 was immunoprecipitated with HA-beads, followed by immunoblotting of co-purified
632 proteins. Asterisk indicates non-specific bands.
633 (E) To narrow down the GMCL1-binding region on 53BP1, sequential 20-amino-acid
634 deletions within the MFF domain were generated. HEK293T cells were co-
635 transfected with EV or FLAG-GMCL1, along with HA-MFF, HA-MFF Δ1410-1430, and
636 site-specific mutants (every three amino acids mutated within 1410–1430 region of
637 53BP1). Immunoprecipitation of 53BP1 was conducted with HA-beads, followed by
638 immunoblotting.
639 (F) HEK293T cells were transfected with FLAG-GMCL1 or FLAG-GMCL2. GMCL1 and
640 GMCL2 were immunoprecipitated with FLAG-beads and analyzed by
641 immunoblotting.
642
643 **Supplemental Figure 2. Mitotic stress imprints apoptotic memory in daughter cells**
644 (A) RNA was extracted from FLAG-GMCL1-expressing U2OS cells (as in Figure 2B). p21
645 and NOXA mRNA levels were quantified by qPCR from three independent
646 experiments. Error bars represent standard deviation.
647 (B) Stable GMCL1 KO U2OS cells were transduced with lentiviruses expressing EV,
648 FLAG-GMCL1 WT, FLAG-GMCL1 EK, or FLAG-GMCL1 RA. Cells were synchronized in
649 M phase, then released into fresh FBS-containing medium for 20 hours following
650 shake-off. Daughter cells were fractionated into soluble and chromatin-bound
651 fractions and analyzed by immunoblotting.
652 (C) RNA was extracted from same cells as in (B), and NOXA and PUMA mRNA levels
653 were quantified by qPCR from three independent experiments. Error bars represent
654 standard deviation.
655 (D) Cell cycle distribution was determined using BrdU pulse and PI staining of
656 asynchronous U2OS WT or FLAG-GMCL1-expressing cells. Error bars represent
657 standard deviation.
658
659 **Supplemental Figure 3. Tissue-specific comparison of GMCL1 gene expression levels**
660 The panel shows GMCL1 expression levels in normal cells and cancer cells based on
661 GENT2[21] . The cells in the bottom table indicate where, GMCL1 expression levels were

662 significantly higher in cancer cells (red), while the blue cells indicate cancers that were
663 previously reported in the literature to exhibit Taxol resistance[13,38].

REFERENCES

1. Hosea, R., Hillary, S., Naqvi, S., Wu, S., and Kasim, V. (2024). The two sides of chromosomal instability: drivers and brakes in cancer. Signal Transduct Target Ther *9*, 75. 10.1038/s41392-024-01767-7.
2. Lens, S.M.A., and Medema, R.H. (2019). Cytokinesis defects and cancer. Nat Rev Cancer *19*, 32-45. 10.1038/s41568-018-0084-6.
3. Lambrus, B.G., and Holland, A.J. (2017). A New Mode of Mitotic Surveillance. Trends Cell Biol *27*, 314-321. 10.1016/j.tcb.2017.01.004.
4. Contadini, C., Monteonofrio, L., Virdia, I., Prodosmo, A., Valente, D., Chessa, L., Musio, A., Fava, L.L., Rinaldo, C., Di Rocco, G., and Soddu, S. (2019). p53 mitotic centrosome localization preserves centrosome integrity and works as sensor for the mitotic surveillance pathway. Cell Death Dis *10*, 850. 10.1038/s41419-019-2076-1.
5. Burigotto, M., Vigorito, V., Gliech, C., Mattivi, A., Ghetti, S., Bisio, A., Lolli, G., Holland, A.J., and Fava, L.L. (2023). PLK1 promotes the mitotic surveillance pathway by controlling cytosolic 53BP1 availability. EMBO Rep *24*, e57234. 10.15252/embr.202357234.
6. Fong, C.S., Mazo, G., Das, T., Goodman, J., Kim, M., O'Rourke, B.P., Izquierdo, D., and Tsou, M.F. (2016). 53BP1 and USP28 mediate p53-dependent cell cycle arrest in response to centrosome loss and prolonged mitosis. Elife *5*. 10.7554/eLife.16270.
7. Meitinger, F., Belal, H., Davis, R.L., Martinez, M.B., Shiau, A.K., Oegema, K., and Desai, A. (2024). Control of cell proliferation by memories of mitosis. Science *383*, 1441-1448. 10.1126/science.add9528.
8. Stracker, T.H. (2024). Regulation of p53 by the mitotic surveillance/stopwatch pathway: implications in neurodevelopment and cancer. Front Cell Dev Biol *12*, 1451274. 10.3389/fcell.2024.1451274.
9. Meitinger, F., Anzola, J.V., Kaulich, M., Richardson, A., Stender, J.D., Benner, C., Glass, C.K., Dowdy, S.F., Desai, A., Shiau, A.K., and Oegema, K. (2016). 53BP1 and USP28 mediate p53 activation and G1 arrest after centrosome loss or extended mitotic duration. J Cell Biol *214*, 155-166. 10.1083/jcb.201604081.
10. Fulcher, L.J., Sobajima, T., Batley, C., Gibbs-Seymour, I., and Barr, F.A. (2025). MDM2 functions as a timer reporting the length of mitosis. Nat Cell Biol. 10.1038/s41556-024-01592-8.
11. Chan, K.S., Koh, C.G., and Li, H.Y. (2012). Mitosis-targeted anti-cancer therapies: where they stand. Cell Death Dis *3*, e411. 10.1038/cddis.2012.148.
12. Giannakakou, P., Robey, R., Fojo, T., and Blagosklonny, M.V. (2001). Low concentrations of paclitaxel induce cell type-dependent p53, p21 and G1/G2 arrest instead of mitotic arrest: molecular determinants of paclitaxel-induced cytotoxicity. Oncogene *20*, 3806-3813. 10.1038/sj.onc.1204487.
13. Gupta, N., Gupta, P., and Srivastava, S.K. (2019). Penfluridol overcomes paclitaxel resistance in metastatic breast cancer. Sci Rep *9*, 5066. 10.1038/s41598-019-41632-0.
14. Baird, R.D., Tan, D.S., and Kaye, S.B. (2010). Weekly paclitaxel in the treatment of recurrent ovarian cancer. Nat Rev Clin Oncol *7*, 575-582. 10.1038/nrclinonc.2010.120.
15. Sosa Iglesias, V., Giuranno, L., Dubois, L.J., Theys, J., and Vooijs, M. (2018). Drug Resistance in Non-Small Cell Lung Cancer: A Potential for NOTCH Targeting? Front Oncol *8*, 267. 10.3389/fonc.2018.00267.

16. Jongens, T.A., Ackerman, L.D., Swedlow, J.R., Jan, L.Y., and Jan, Y.N. (1994). Germ cell-less encodes a cell type-specific nuclear pore-associated protein and functions early in the germ-cell specification pathway of Drosophila. Genes Dev *8*, 2123-2136. 10.1101/gad.8.18.2123.
17. Jongens, T.A., Hay, B., Jan, L.Y., and Jan, Y.N. (1992). The germ cell-less gene product: a posteriorly localized component necessary for germ cell development in Drosophila. Cell *70*, 569-584. 10.1016/0092-8674(92)90427-e.
18. Liebe, B., Petukhova, G., Barchi, M., Bellani, M., Braselmann, H., Nakano, T., Pandita, T.K., Jasin, M., Fornace, A., Meistrich, M.L., et al. (2006). Mutations that affect meiosis in male mice influence the dynamics of the mid-preleptotene and bouquet stages. Exp Cell Res *312*, 3768-3781. 10.1016/j.yexcr.2006.07.019.
19. Liu, X.X., Cai, L., and Liu, F.J. (2018). An in silico analysis of human sperm genes associated with asthenozoospermia and its implication in male infertility. Medicine (Baltimore) *97*, e13338. 10.1097/MD.0000000000013338.
20. Consortium, G. (2020). The GTEx Consortium atlas of genetic regulatory effects across human tissues. Science *369*, 1318-1330. 10.1126/science.aaz1776.
21. Park, S.J., Yoon, B.H., Kim, S.K., and Kim, S.Y. (2019). GENT2: an updated gene expression database for normal and tumor tissues. BMC Med Genomics *12*, 101. 10.1186/s12920-019-0514-7.
22. Pae, J., Cinalli, R.M., Marzio, A., Pagano, M., and Lehmann, R. (2017). GCL and CUL3 Control the Switch between Cell Lineages by Mediating Localized Degradation of an RTK. Dev Cell *42*, 130-142.e137. 10.1016/j.devcel.2017.06.022.
23. Bonchuk, A., Balagurov, K., and Georgiev, P. (2023). BTB domains: A structural view of evolution, multimerization, and protein-protein interactions. Bioessays *45*, e2200179. 10.1002/bies.202200179.
24. Holm, L. (2022). Dali server: structural unification of protein families. Nucleic Acids Res *50*, W210-W215. 10.1093/nar/gkac387.
25. Usher, E.T., Sabri, N., Rohac, R., Boal, A.K., Mittag, T., and Showalter, S.A. (2021). Intrinsically disordered substrates dictate SPOP subnuclear localization and ubiquitination activity. J Biol Chem *296*, 100693. 10.1016/j.jbc.2021.100693.
26. Abramson, J., Adler, J., Dunger, J., Evans, R., Green, T., Pritzel, A., Ronneberger, O., Willmore, L., Ballard, A.J., Bambrick, J., et al. (2024). Accurate structure prediction of biomolecular interactions with AlphaFold 3. Nature *630*, 493-500. 10.1038/s41586-024-07487-w.
27. Panier, S., and Boulton, S.J. (2014). Double-strand break repair: 53BP1 comes into focus. Nat Rev Mol Cell Biol *15*, 7-18. 10.1038/nrm3719.
28. Cong, L., Ran, F.A., Cox, D., Lin, S., Barretto, R., Habib, N., Hsu, P.D., Wu, X., Jiang, W., Marraffini, L.A., and Zhang, F. (2013). Multiplex genome engineering using CRISPR/Cas systems. Science *339*, 819-823. 10.1126/science.1231143.
29. Corsello, S.M., Nagari, R.T., Spangler, R.D., Rossen, J., Kocak, M., Bryan, J.G., Humeidi, R., Peck, D., Wu, X., Tang, A.A., et al. (2020). Discovering the anti-cancer potential of non-oncology drugs by systematic viability profiling. Nat Cancer *1*, 235-248. 10.1038/s43018-019-0018-6.

751 30. Chen, X., Zhang, T., Su, W., Dou, Z., Zhao, D., Jin, X., Lei, H., Wang, J., Xie, X., Cheng, B., et
752 al. (2022). Mutant p53 in cancer: from molecular mechanism to therapeutic modulation.
753 Cell Death Dis *13*, 974. 10.1038/s41419-022-05408-1.
754 31. Zhao, B., Rothenberg, E., Ramsden, D.A., and Lieber, M.R. (2020). The molecular basis
755 and disease relevance of non-homologous DNA end joining. Nat Rev Mol Cell Biol *21*,
756 765-781. 10.1038/s41580-020-00297-8.
757 32. Wang, D., Ma, J., Botuyan, M.V., Cui, G., Yan, Y., Ding, D., Zhou, Y., Krueger, E.W., Pei, J.,
758 Wu, X., et al. (2021). ATM-phosphorylated SPOP contributes to 53BP1 exclusion from
759 chromatin during DNA replication. Sci Adv *7*. 10.1126/sciadv.abd9208.
760 33. Han, X., Zhang, L., Chung, J., Mayca Pozo, F., Tran, A., Seachrist, D.D., Jacobberger, J.W.,
761 Keri, R.A., Gilmore, H., and Zhang, Y. (2014). UbcH7 regulates 53BP1 stability and DSB
762 repair. Proc Natl Acad Sci U S A *111*, 17456-17461. 10.1073/pnas.1408538111.
763 34. Kucharski, T.J., Minshall, P.E., Moustafa-Kamal, M., Turnell, A.S., and Teodoro, J.G. (2017).
764 Reciprocal Regulation between 53BP1 and the Anaphase-Promoting Complex/Cyclosome
765 Is Required for Genomic Stability during Mitotic Stress. Cell Rep *18*, 1982-1995.
766 10.1016/j.celrep.2017.01.080.
767 35. Rona, G., Miwatani-Minter, B., Zhang, Q., Goldberg, H.V., Kerzhnerman, M.A., Howard,
768 J.B., Simoneschi, D., Lane, E., Hobbs, J.W., Sassani, E., et al. (2024). CDK-independent role
769 of D-type cyclins in regulating DNA mismatch repair. Mol Cell.
770 10.1016/j.molcel.2024.02.010.
771 36. Rona, G., Roberti, D., Yin, Y., Pagan, J.K., Homer, H., Sassani, E., Zeke, A., Busino, L.,
772 Rothenberg, E., and Pagano, M. (2018). PARP1-dependent recruitment of the FBXL10-
773 RNF68-RNF2 ubiquitin ligase to sites of DNA damage controls H2A.Z loading. Elife *7*.
774 10.7554/eLife.38771.
775 37. Clijsters, L., Hoencamp, C., Calis, J.J.A., Marzio, A., Handgraaf, S.M., Cuitino, M.C.,
776 Rosenberg, B.R., Leone, G., and Pagano, M. (2019). Cyclin F Controls Cell-Cycle
777 Transcriptional Outputs by Directing the Degradation of the Three Activator E2Fs. Mol
778 Cell *74*, 1264-1277.e1267. 10.1016/j.molcel.2019.04.010.
779 38. Alalawy, A.I. (2024). Key genes and molecular mechanisms related to Paclitaxel
780 Resistance. Cancer Cell Int *24*, 244. 10.1186/s12935-024-03415-0.
781

Figure 1

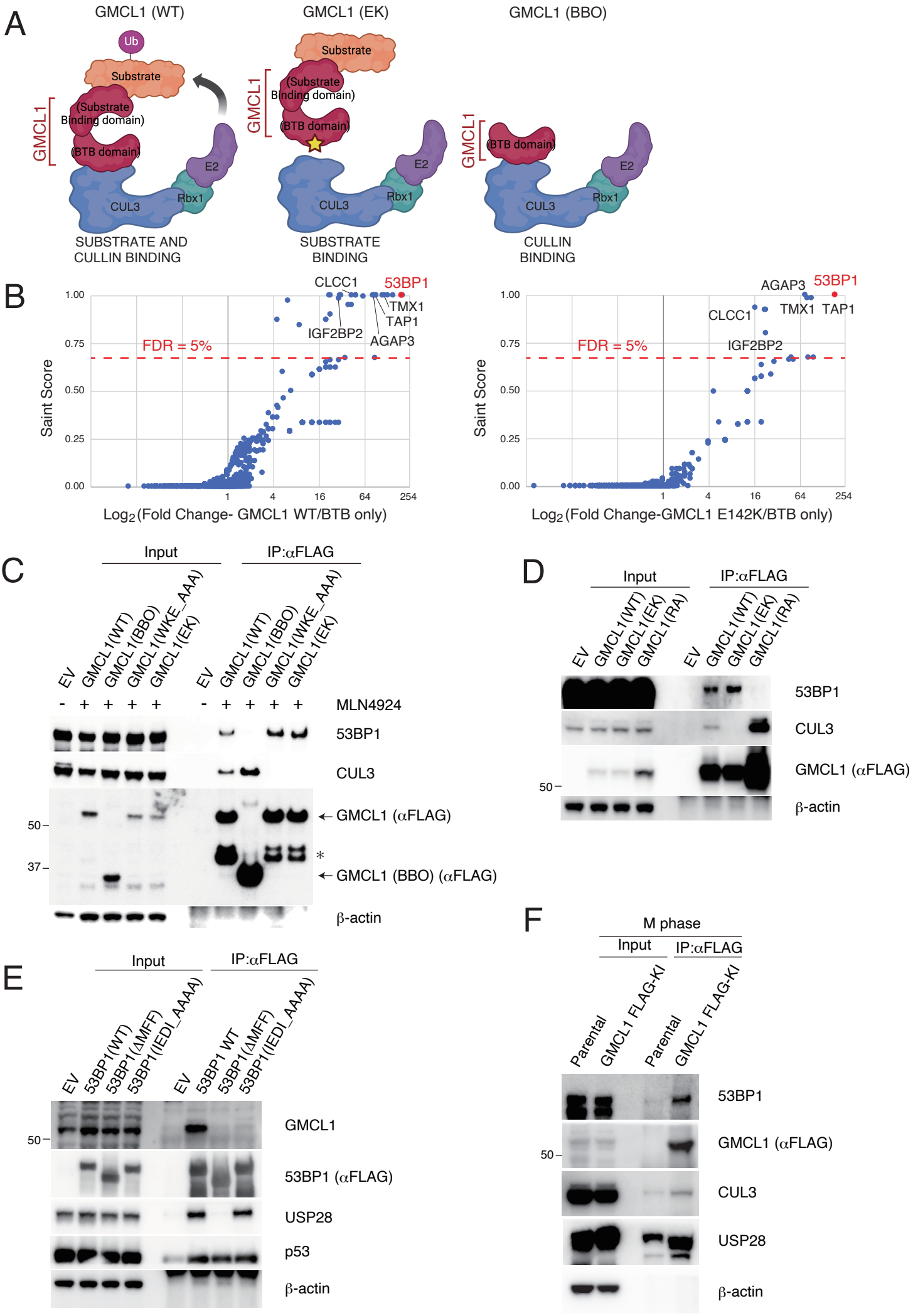
A
GMCL1 (WT)
GMCL1 (EK)
GMCL1 (BBO)
Ub
Substrate
(Substrate Binding domain)
(BTB domain)
GMCL1
E2
Rbx1
CUL3
SUBSTRATE AND CULLIN BINDING
SUBSTRATE BINDING
CULLIN BINDING
B
Saint Score
FDR = 5%
CLCC1
53BP1
TMX1
TAP1
IGF2BP2
AGAP3
Log2(Fold Change- GMCL1 WT/BTB only)
Log2(Fold Change-GMCL1 E142K/BTB only)
C
Input
IP:αFLAG
EV
GMCL1(WT)
GMCL1(BBO)
GMCL1(WKE_AAA)
GMCL1(EK)
MLN4924
53BP1
CUL3
GMCL1 (αFLAG)
GMCL1 (BBO) (αFLAG)
β-actin
D
GMCL1(RA)
E
53BP1(WT)
53BP1(ΔMFF)
53BP1(IEDI_AAAA)
53BP1 WT
GMCL1
53BP1 (αFLAG)
USP28
p53
F
M phase
Parental
GMCL1 FLAG-KI

Supplemental Figure1

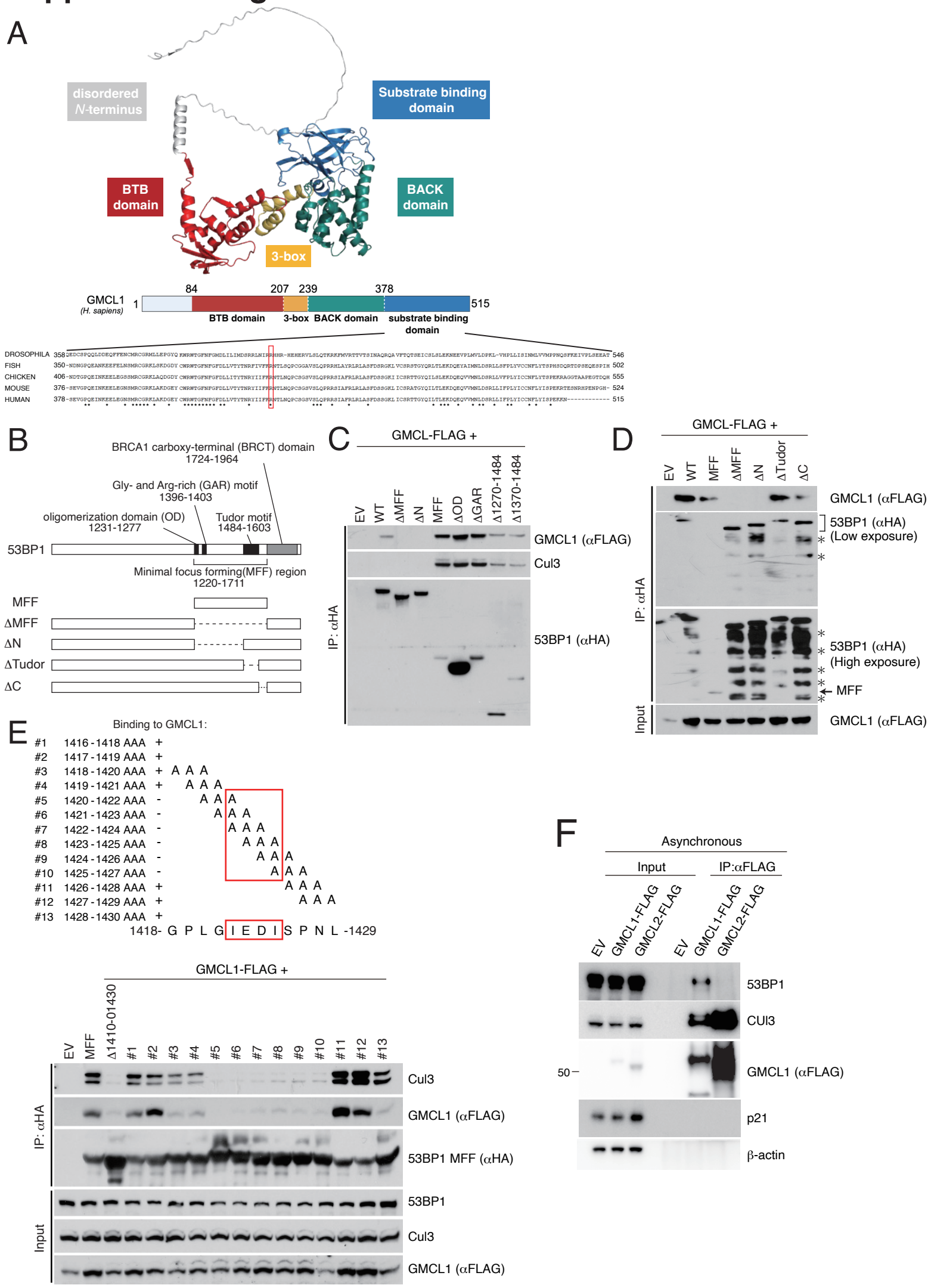

Figure 2

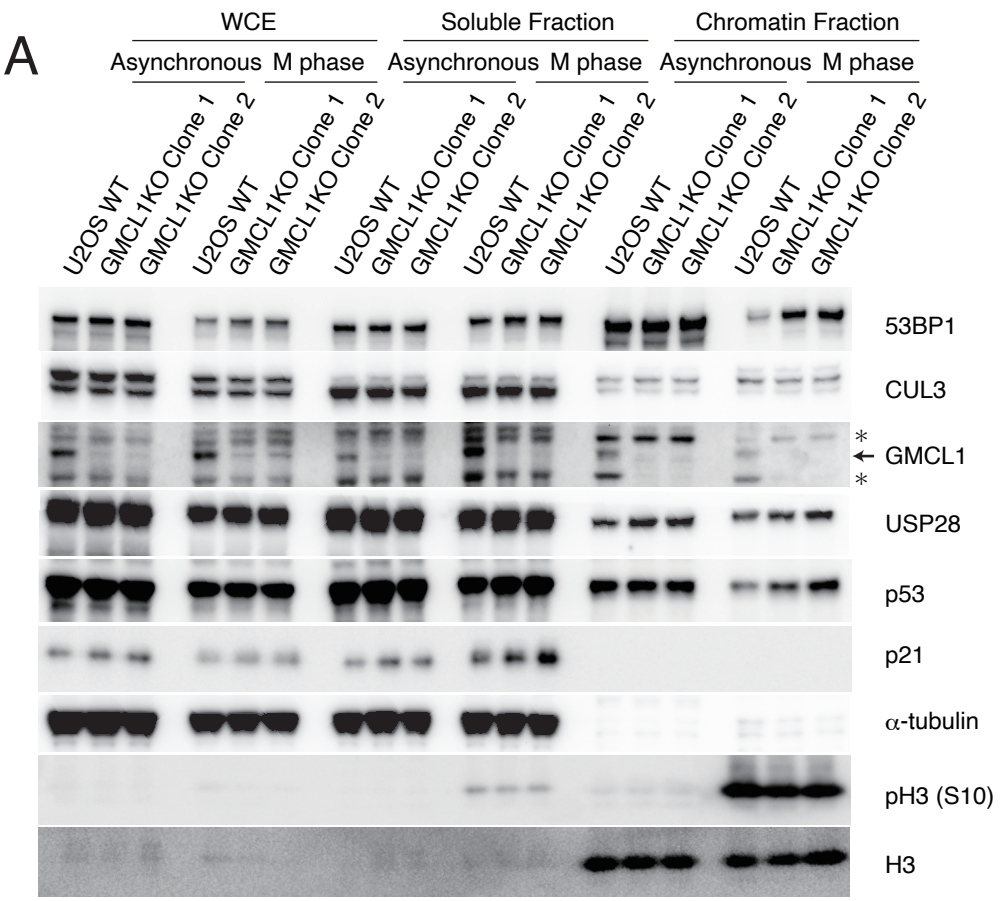
A
WCE
Soluble Fraction
Chromatin Fraction
Asynchronous
M phase
U2OS WT
GMCL1KO Clone 1
GMCL1KO Clone 2
53BP1
CUL3
GMCL1
USP28
p53
p21
α-tubulin
pH3 (S10)
H3

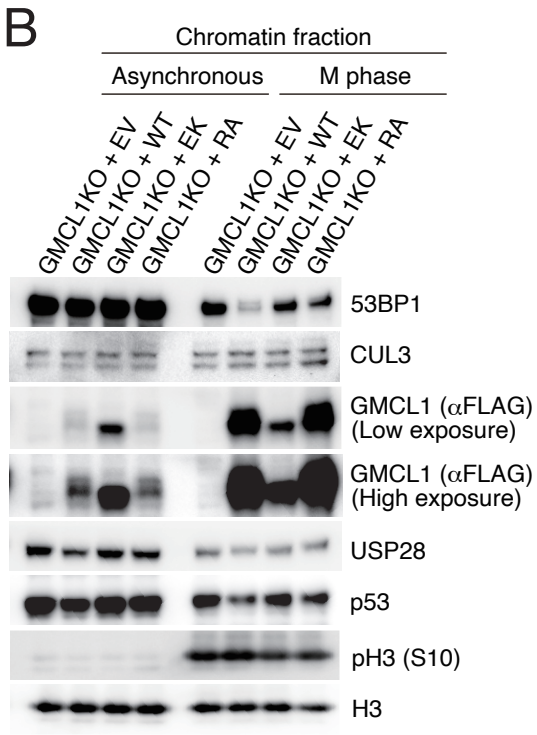
B
Chromatin fraction
Asynchronous
M phase
GMCL1KO + EV
GMCL1KO + WT
GMCL1KO + EK
GMCL1KO + RA
53BP1
CUL3
GMCL1 (αFLAG)
(Low exposure)
GMCL1 (αFLAG)
(High exposure)
USP28
p53
pH3 (S10)
H3

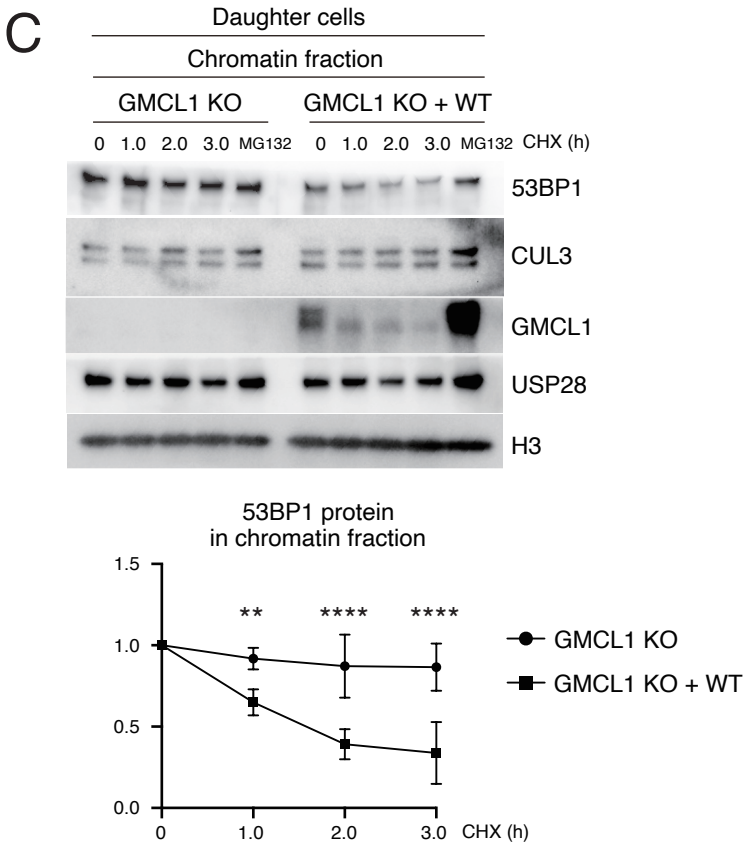
C
Daughter cells
Chromatin fraction
GMCL1 KO
GMCL1 KO + WT
0 1.0 2.0 3.0 MG132
CHX (h)
53BP1
CUL3
GMCL1
USP28
H3
53BP1 protein
in chromatin fraction
1.5
1.0
0.5
0.0
**
****
****
GMCL1 KO
GMCL1 KO + WT
0
1.0
2.0
3.0
CHX (h)

Supplemental Figure 2

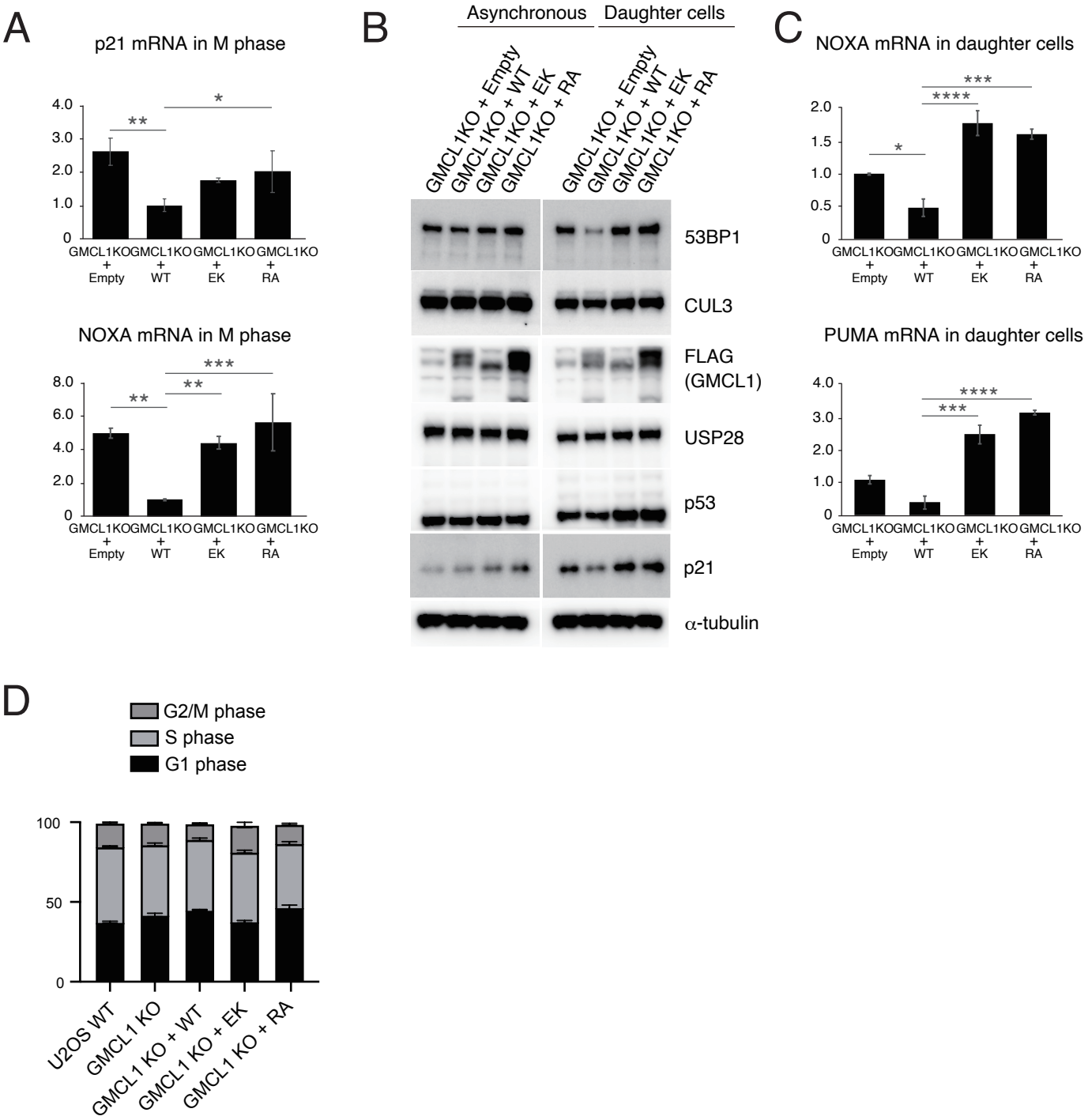

Figure 3

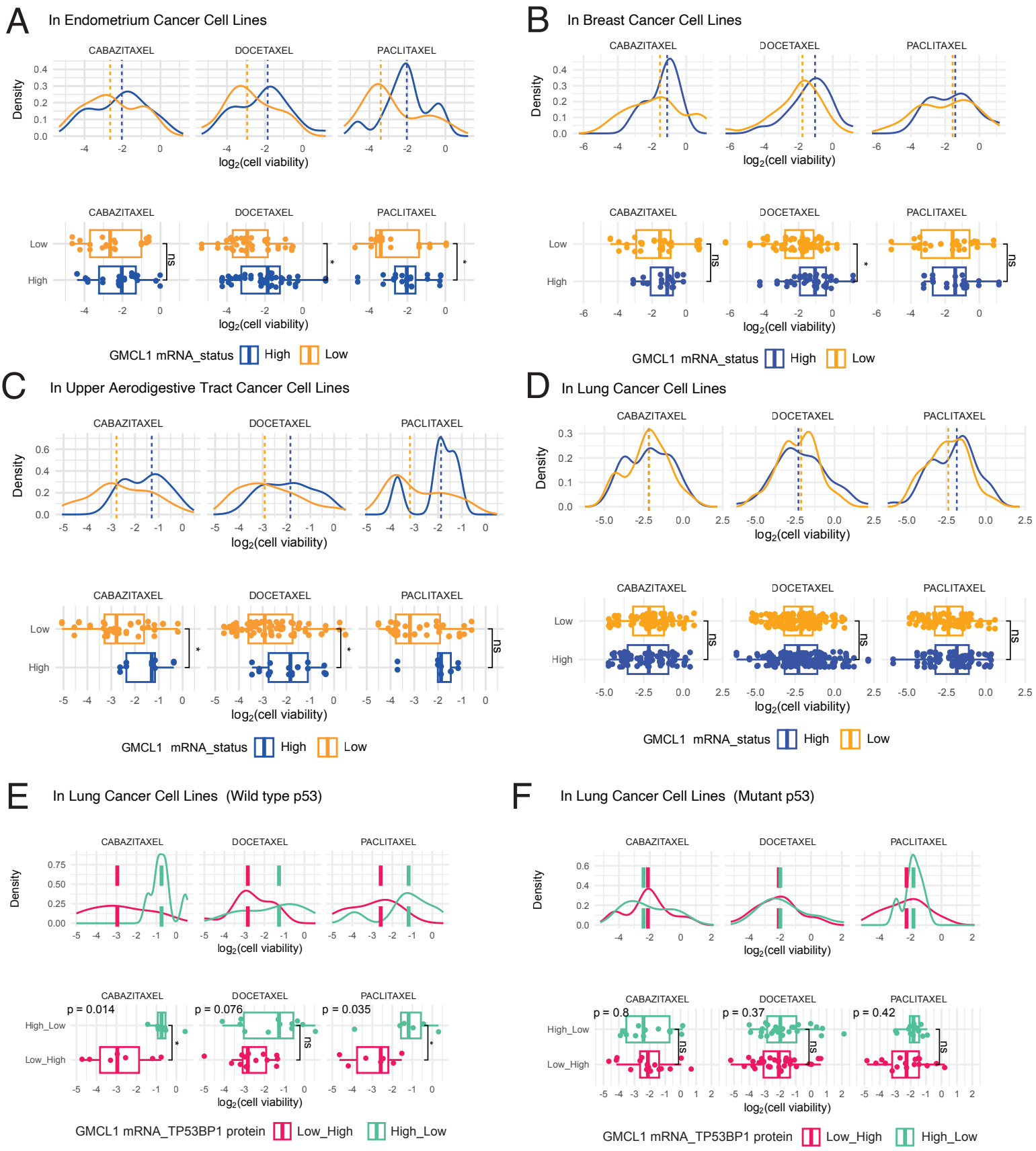
A
In Endometrium Cancer Cell Lines
B
In Breast Cancer Cell Lines
C
In Upper Aerodigestive Tract Cancer Cell Lines
D
In Lung Cancer Cell Lines
E
In Lung Cancer Cell Lines (Wild type p53)
F
In Lung Cancer Cell Lines (Mutant p53)
CABAZITAXEL
DOCETAXEL
PACLITAXEL
Density
log2(cell viability)
Low
High
ns
*
GMCL1 mRNA_status
High
Low
p = 0.014
p = 0.076
p = 0.035
p = 0.8
p = 0.37
p = 0.42
High_Low
Low_High
GMCL1 mRNA_TP53BP1 protein

Supplemental Figure 3

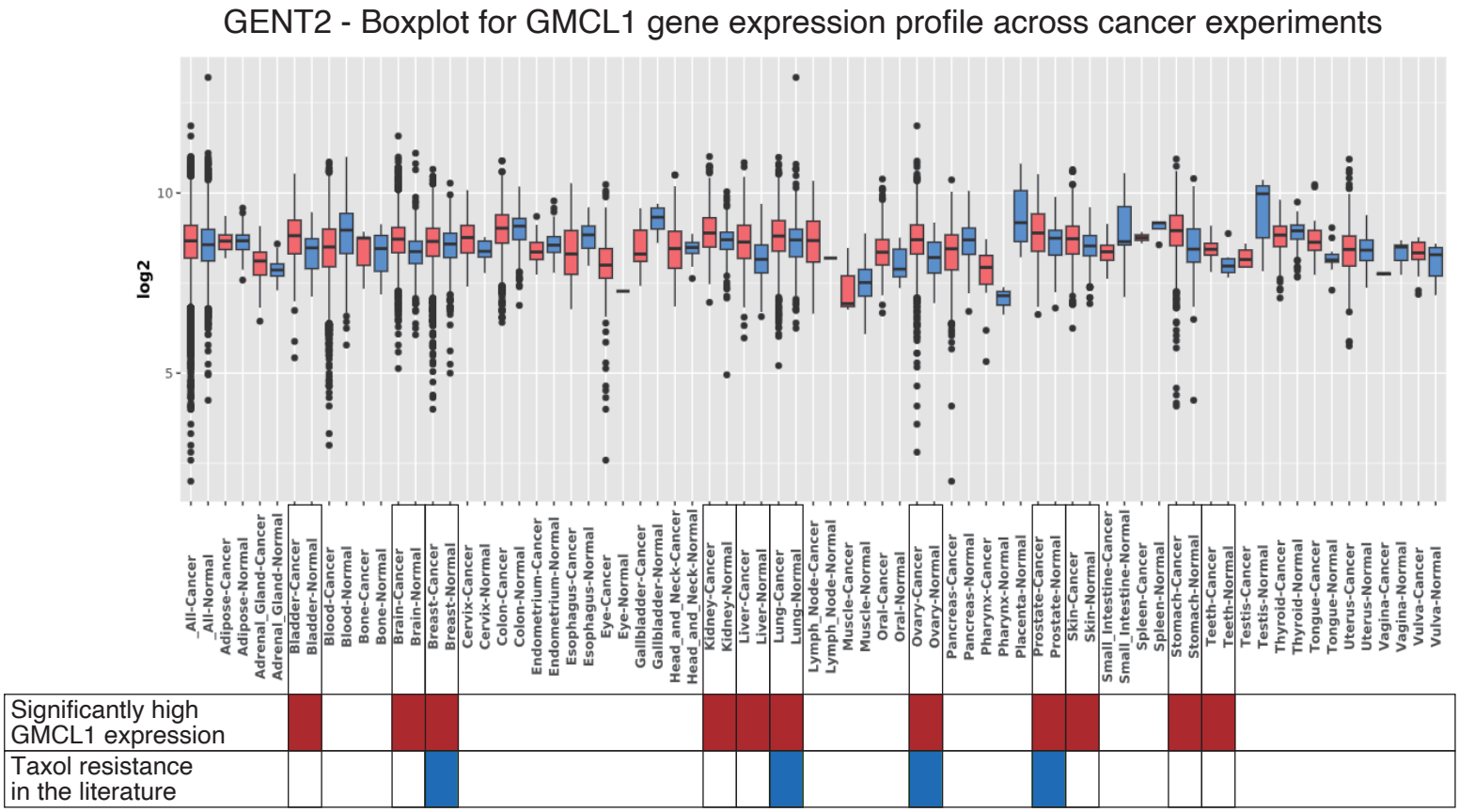

Figure 4

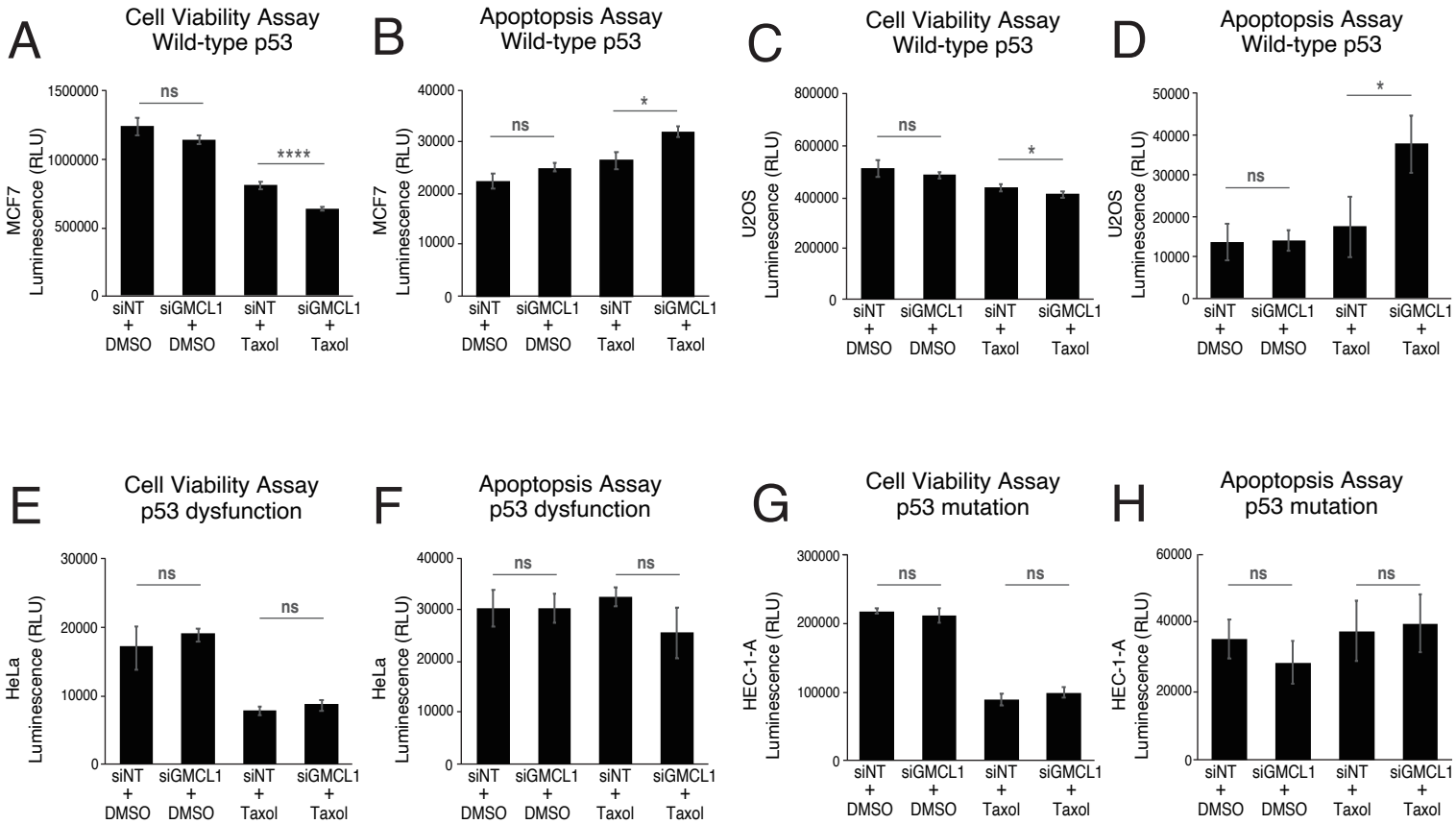
A
Cell Viability Assay
Wild-type p53
MCF7
Luminescence (RLU)
1500000
1000000
500000
0
ns
****
siNT + DMSO
siGMCL1 + DMSO
siNT + Taxol
siGMCL1 + Taxol
B
Apoptopsis Assay
Wild-type p53
MCF7
Luminescence (RLU)
40000
30000
20000
10000
0
ns
*
siNT + DMSO
siGMCL1 + DMSO
siNT + Taxol
siGMCL1 + Taxol
C
Cell Viability Assay
Wild-type p53
U2OS
Luminescence (RLU)
800000
600000
400000
200000
0
ns
*
siNT + DMSO
siGMCL1 + DMSO
siNT + Taxol
siGMCL1 + Taxol
D
Apoptopsis Assay
Wild-type p53
U2OS
Luminescence (RLU)
50000
40000
30000
20000
10000
0
ns
*
siNT + DMSO
siGMCL1 + DMSO
siNT + Taxol
siGMCL1 + Taxol
E
Cell Viability Assay
p53 dysfunction
HeLa
Luminescence (RLU)
30000
20000
10000
0
ns
ns
siNT + DMSO
siGMCL1 + DMSO
siNT + Taxol
siGMCL1 + Taxol
F
Apoptopsis Assay
p53 dysfunction
HeLa
Luminescence (RLU)
40000
30000
20000
10000
0
ns
ns
siNT + DMSO
siGMCL1 + DMSO
siNT + Taxol
siGMCL1 + Taxol
G
Cell Viability Assay
p53 mutation
HEC-1-A
Luminescence (RLU)
300000
200000
100000
0
ns
ns
siNT + DMSO
siGMCL1 + DMSO
siNT + Taxol
siGMCL1 + Taxol
H
Apoptopsis Assay
p53 mutation
HEC-1-A
Luminescence (RLU)
60000
40000
20000
0
ns
ns
siNT + DMSO
siGMCL1 + DMSO
siNT + Taxol
siGMCL1 + Taxol

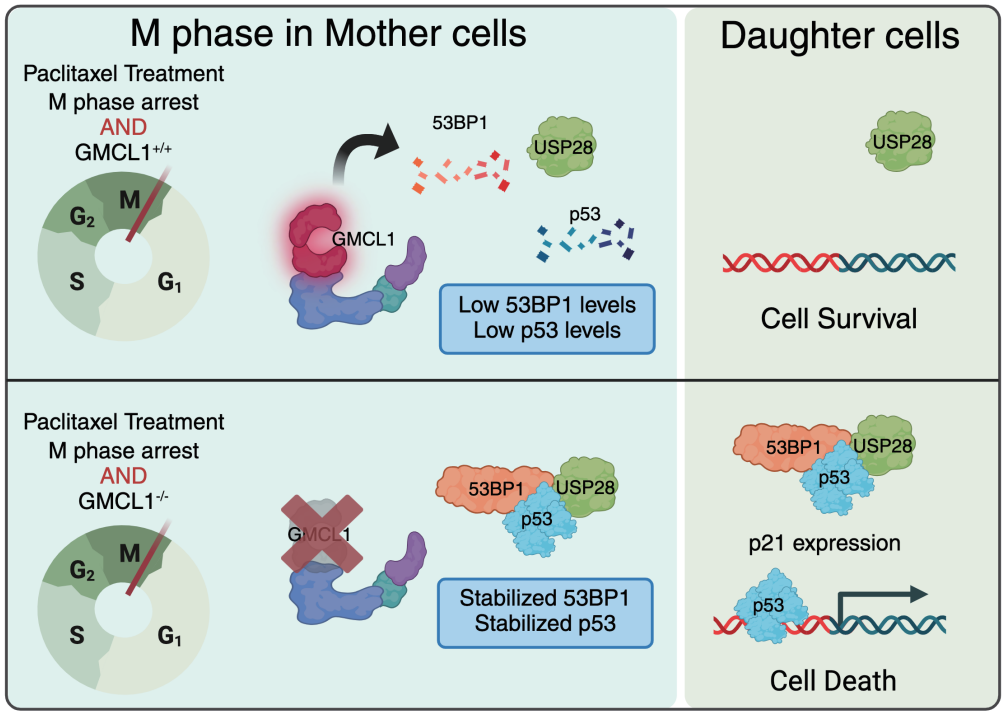
I
M phase in Mother cells
Daughter cells
Paclitaxel Treatment
M phase arrest
AND
GMCL1+/+
M
G2
S
G1
53BP1
USP28
p53
GMCL1
Low 53BP1 levels
Low p53 levels
USP28
Cell Survival
Paclitaxel Treatment
M phase arrest
AND
GMCL1-/-
M
G2
S
G1
GMCL1
53BP1
USP28
p53
Stabilized 53BP1
Stabilized p53
53BP1
USP28
p53
p21 expression
p53
Cell Death